Plant Direct

WILEY | American Society of Plant Biologists SEB SOCIETY FOR EXPERIMENTAL BIOLOGY

RESEARCH ARTICLE OPEN ACCESS

Virus-Induced Gene Silencing in *Calendula officinalis* (Pot Marigold)

Daria Cuthbert[1] | Connor Tansley[2] | Melissa Salmon[1] | Nicola Patron[2]

[1]Earlham Institute, Norwich, UK | [2]Department of Plant Sciences, University of Cambridge, Cambridge, UK

Correspondence: Connor Tansley (ct677@cam.ac.uk) | Nicola Patron (njp56@cam.ac.uk)

Received: 19 December 2025 | **Revised:** 14 April 2026 | **Accepted:** 13 May 2026

Keywords: agroinfiltration | Asteraceae | cycloartenol | phytosterols | virus-induced gene silencing

ABSTRACT

Virus-induced gene silencing (VIGS) is a method that exploits plant antiviral defense mechanisms to downregulate endogenous genes. The technique is versatile, rapid, and widely used for functional genomics studies. Here, we report a method for VIGS in the medicinal plant, *Calendula officinalis* (pot marigold). This species produces anti-inflammatory triterpenoids and has also been bred and cultivated as an ornamental plant. We describe a method for the injection of *Agrobacterium tumefaciens* cultures into leaf midribs and compare visual marker genes for tracking VIGS utilizing constructs that simultaneously target visual marker and target genes. We use these tools to demonstrate that silencing a gene encoding cycloartenol synthase results in changes to leaf phytosterols. This method could be used to further investigate the genetic basis of specialized metabolism in this species and could be adapted to other members of the Asteraceae family, many of which are of economic and chemical value.

1 | Introduction

RNA silencing is a key mechanism for regulating gene expression in eukaryotes in which epigenetic modifications are made to DNA sequences (transcriptional gene silencing [TGS]) or messenger RNAs (mRNAs) are degraded or prevented from translating (posttranscriptional gene silencing [PTGS]) (Zhang et al. 2015; Zhan and Meyers 2023). In plants, RNA silencing is also used for antiviral immunity. In this process, viral double-stranded RNAs (dsRNAs) are cleaved into small interfering RNAs (siRNAs) that bind to members of the argonaute (AGO) protein family and are incorporated into RNA-induced silencing complexes (RISC) where they serve as guides for the cleavage or translational suppression of viral RNAs (Lopez-Gomollon and Baulcombe 2022). This process, known as virus-induced gene silencing (VIGS), has been adapted to enable the silencing of endogenous genes for functional studies and biotechnological applications.

VIGS typically employs *A. tumefaciens* to deliver viral vectors encoding viral proteins and short (~300 bp) sequences of the target gene. A critical factor is the host range of the viral vector. Over the past years, multiple plant viruses (e.g., tobacco mosaic virus [TMV], potato virus X [PVX], and tomato golden mosaic virus [TGMV]) have been used to develop VIGS vectors. Of these, tobacco rattle virus (TRV) has the broadest host range, with results reported from numerous angiosperms (Dommes et al. 2019). To facilitate the development of VIGS methods in new species and to test the efficacy of VIGS vectors, genes of which silencing results in an easily visible phenotype are employed. Commonly used genes include *phytoene desaturase* (*PDS*), of which downregulation disrupts the conversion of phytoene to ζ-carotene, and *magnesium chelatase subunit H* (*CHL-H*), the product of which is required for the conversion of protoporphyrinogen IX to Mg-protoporphyrin IX in chlorophyll biosynthesis (Ratcliff et al. 2001; Hiriart et al. 2003). The downregulation of these genes results in white or yellow leaves (Ratcliff et al. 2001; Hiriart et al. 2003).

Daria Cuthbert and Connor Tansley contributed equally to this work.

This is an open access article under the terms of the Creative Commons Attribution License, which permits use, distribution and reproduction in any medium, provided the original work is properly cited.

© 2026 The Author(s). *Plant Direct* published by American Society of Plant Biologists and the Society for Experimental Biology and John Wiley & Sons Ltd.

VIGS has been widely used in model plants such as *Nicotiana benthamiana* (Kumagai et al. 1995; Hiriart et al. 2003) and *Arabidopsis thaliana* (thale cress) (Burch-Smith et al. 2006). It has also been utilized in several crops, including *Hordeum vulgare* (barley) (Hein et al. 2005), *Oryza sativa* (rice) (Ding et al. 2007), *Zea mays* (maize) (Wang et al. 2016), and *Gossypium* (cotton) species (Tian et al. 2024). Furthermore, it has been successfully applied to woody species including *Malus* × *domestica* L (apple) (Navarro Gallón et al. 2017), *Pyrus* spp. (pear) (Ni et al. 2023), and *Paeonia rockii* (tree peony) (Yang et al. 2025). VIGS has been employed to study numerous gene families, including those involved in primary and secondary metabolism (Zulfiqar et al. 2023). Several studies have reported the use of VIGS for the discovery and characterization of genes involved in the biosynthesis of bioactives and natural products. For example, VIGS was used to discover and characterize genes involved in the production of terpenoid indole alkaloids in *Catharanthus roseus* (Madagascar periwinkle) (Liscombe and O'Connor 2011; Yamamoto et al. 2021). It has also been used to investigate the function of genes encoding cytochrome P450s involved in the production of ursolic and oleanolic acids in *Ocimum basilicum* (sweet basil) (Misra et al. 2020). VIGS is particularly useful for studying genes involved in the biosynthesis of compounds that are essential for plant growth and development, such as the role of cycloartenol synthases (CASs), of which loss-of-function early in development results in severe phenotypes or lethality (Babiychuk et al. 2008). The use of VIGS to silence *SlCAS* in *Solanum lycopersicum* (tomato) enabled the elucidation of cholesterol biogenesis (Sonawane et al. 2016). In that study, silencing of *SlCAS* led to a significant decrease in α-tomatine, cholesterol, stigmasterol, β-sitosterol, isofucosterol, and cycloartenol. At the same time, the level of β-amyrin, which depends on the availability of the 2,3-oxidosqualene precursor, significantly increased in the leaves of plants in which *SlCAS was* silenced.

The Asteraceae family is the largest and most diverse family of land plants. However, methods for gene delivery and genetic transformation are limited to a few species (Darqui et al. 2021). Stable transformation has been demonstrated in the Asteraceae crop species, *Lactuca sativa* (lettuce), *Helianthus annus* (sunflower) (Müller et al. 2001; Darqui et al. 2021; Roche et al. 2025), and, the medicinal plant, *Artemisia annua* (sweet wormwood) (Alam et al. 2014; Elfahmi et al. 2014; Hassani et al. 2023). VIGS has been demonstrated in common sunflower, sweet wormwood, lettuce (Mardini et al. 2024; Wang et al. 2021; Liu et al. 2024) and has also been used to study anthocyanin biosynthesis in *Gerbera hybrida* (African daisy) (Deng et al. 2012) and chlorogenic acid and dicaffeoylquinic acid production in *Cynara cardunculus* (globe artichoke) (Moglia et al. 2016). The Asteraceae species, *Calendula officinalis* (pot marigold), has been used as a medicinal plant for thousands of years. Recently, we have shown that hydroxylated triterpenoids found in these species have potent anti-inflammatory activity (Golubova et al. 2025). To date, few studies have aimed at genetic transformation of pot marigold; however, *Rhizobium rhizogenes* has been used to produce transgenic hairy root cultures (Długosz et al. 2018; Matvieieva et al. 2025). Here, we report the development of methods for *A. tumefaciens* infiltration and VIGS for this species, applying them to silence *CAS*.

2 | Results

2.1 | *A. tumefaciens*-Mediated Transient Gene Expression

We first investigated whether pot marigold is amenable to transient transfection by *A. tumefaciens*. To do this we transformed three *A. tumefaciens* strains (GV3101, LBA4404, and AGL1) with a binary vector (pEPCTαKN0001; Table S1) encoding a chimeric gene for constitutive expression of firefly luciferase (LucF) under control of the Cauliflower Mosaic Virus 35s promoter (CaMV35sP). The resulting *A. tumefaciens* strains were infiltrated into the abaxial side of leaves of young (28 days after germination) pot marigold and *N. benthamiana* (control) plants using a 1 mL needleless syringe. Five days after infiltration, protein was extracted and luminescence was quantified. In *N. benthamiana*, *A. tumefaciens* LBA4404 gave the highest levels of luminescence (Figure 1 and Table S2). Expectedly, levels of luminescence detected in pot marigold were lower than

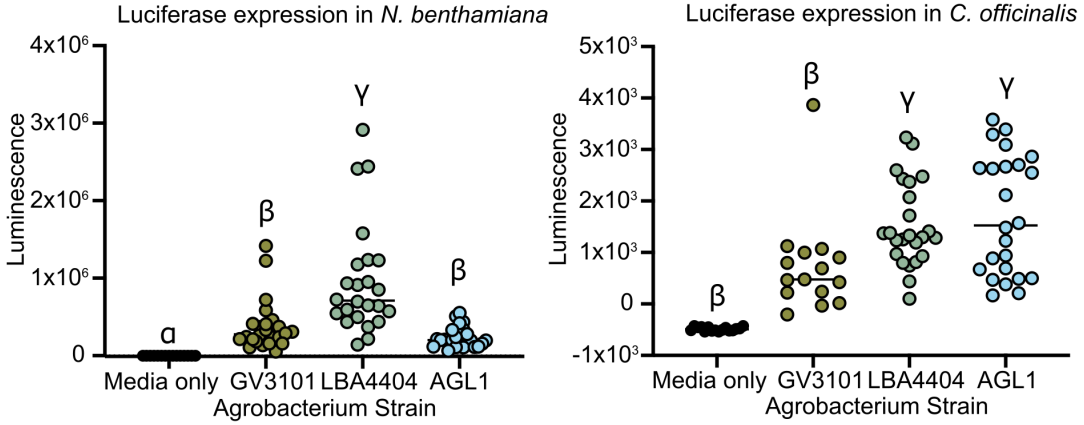


FIGURE 1 | **Transient expression of luciferase reporters in *Nicotiana benthamiana* and *Calendula officinalis* (pot marigold).** Leaves were infiltrated with *Agrobacterium tumefaciens* GV3101, LBA4404, and AGL1 carrying constructs for constitutive expression of firefly luciferase (LucF). Eight leaf disks were sampled from each of three independently infiltrated plants, except pot marigold GV3101 (two plants). Dots represent individual leaf discs. Significant differences were analyzed using a Kruskal–Wallis test with a post hoc Dunn test into groupings represented by α, β, or γ.

those observed in *N. benthamiana* (three orders of magnitude). Nevertheless, significant levels of luminescence were detected in plants infiltrated with *A. tumefaciens* AGL1 and *A. tumefaciens* LBA4404 (Figure 1 and Table S2). *A. tumefaciens* AGL1 gave the highest levels of expression and was used in subsequent experiments.

2.2 | Development of a Visual Marker for Virus-Induced Gene Silencing in Pot Marigold

Next, we identified pot marigold orthologues of *PDS* and *CHL-H* to evaluate their use as visual marker genes for VIGS. To identify candidates, previously characterized *PDS* and *CHL-H* genes from *Nicotiana* sp. (*NbPDS*; LC543532.1 and *NtCHL-H;* NM_001325713.1) were used as queries in tBLASTn to search existing pot marigold genome and transcriptome sequence data (GCA_964273985.1; PRJEB80524). Two candidate *CoPDS* genes were identified encoding proteins with 96.5% identity to each other. Three candidate *CoCHL-H* genes were identified encoding proteins with 97.5%–98.8% identity to each other. The translated amino acid sequences of these genes were used to search the predicted translatomes of five Asteraceae species (*Helianthus annuus*, *Cynara cardunculus* var. scolymus, *Artemisia annua*, *Lactuca sativa*, and *Cichorium endivia)* and three non-Asteraceae (*Arabidopsis thaliana*, *N. benthamiana*, and *Amborella trichopoda*). *H. annuus, C. cardunculus* var. scolymus, *L. sativa, A. thaliana*, and *N. benthamiana PDS* genes have previously been silenced through VIGS. *A. annua*, *A. thaliana*, *N. benthamiana CHL-H* genes have also been silenced through VIGS. *A. trichopoda* was included as an outgroup as an early diverging flowering plant. *C. endivia* was included to increase the resolution of the Asteraceae. The retrieved sequences were used to construct a maximum likelihood phylogeny in which CoPDS and CoCHL candidates were observed to be most closely related to candidates from other Asteraceae (Figure 2A). To confirm which of the candidate visual selectable marker genes were expressed in our target tissues (leaves and flowers), we investigated the expression levels of *CoPDS and CoCHL* genes in three tissues of pot marigold by differential gene expression analysis of a previously published RNAseq dataset of three tissues, leaves, ray florets, and disk florets (https://doi.org/10.5281/zenodo.13869958, DESeq2, Salmon v1.2.0; Golubova et al. 2025). Both *CoPDS1 and CoPDS2* were most highly expressed in pot marigold ray florets. Expression was also detected in the leaves (Figure 2B). All *CoCHL-H* genes were found to be predominantly expressed in leaves with minimal expression in floral tissues. This is expected because of its role in chlorophyll biosynthesis. *CoCHL-H2* and *3* were the most highly expressed (Figure 2B).

The pTRV vectors are known to have the widest host range of established VIGS vectors and thus were selected for use. The two *CoPDS genes* share a 291 bp region in which there is only a single nucleotide polymorphism (SNP). This region was amplified and cloned into pTRV2-GG (Addgene plasmid # 105349; Table S1). Similarly, 303 bp fragments of *CoCHL-H1, CoCHL-H2*, and *CoCHL-H3* were amplified and cloned into pTRV2-GG (Addgene plasmid # 105349; Table S1). Plants were co-infiltrated at 28 days old with a strain of *A. tumefaciens* AGL1 containing pTRV1 and a strain containing pTRV2 into which fragments of the visual marker genes described above had been cloned (pTRV2-*PDS_1/2*, pTRV2-*CoCHL-H1*, pTRV2-*CHL-H_2*, and pTRV2-*CoCHL-H_3*). We initially compared leaf infiltration with a 1-mL needless syringe to injection with a needle into the primary veins (midribs) of the first true leaf of 28-day-old plants (Data S1). In plants in which leaf infiltration was used, only minimal loss of green pigment was observed around the site of infiltration, and no further analyses were performed on these plants. In plants in which pTRV-*PDS*, pTRV-*CHL-H_1*, or pTRV-*CHL-H_2* was injected into the midrib, a bleaching phenotype was observed approximately 35 days after infiltration (dpi) in newly developed leaves. Surprisingly, given the comparatively low level of *CoCHL-H1* expression, plants in which *CoCHL-H1* were targeted showed the most robust visual phenotype of the three *CoCHL-H* candidates (Figure 2C). However, *CoPDS* showed the most obvious phenotype and was selected for subsequent assays (Figure 2C,D).

In previous studies, infiltration with *A. tumefaciens* carrying an empty pTRV2 vector was shown to result in increased viral symptoms. In contrast, vectors in which a 300 bp fragment of a GFP coding sequence was used showed no symptoms (Wu et al. 2011; Broderick and Jones 2014). Thus, an "empty vector" control VIGS vector with a visual marker was constructed by fusing the previously tested fragment of *CoPDS* to a 300 bp fragment of GFP, creating pTRV2(PDS:GFP). The efficacy of this vector was tested by co-infiltration with pTRV1 into plants as previously described. Thirty-eight days after infiltration, RNA was extracted from leaf tissues in which the leaves showed a bleaching phenotype and the expression level of two reference genes (*SAND* and *PROTEIN PHOSPHATASE 2A [PP2A]*), the target genes *CoPDS1 and CoPDS2*, and the TRV capsid protein gene were assessed by qRT-PCR. Transcripts of the TRV capsid protein gene were only detected in tissues infiltrated with TRV vectors (Figure S1 and Table S3). Infiltration with pTRV1 + pTRV2(PDS:GFP) reduced the expression of *CoPDS1* (92.1%) and *CoPDS2* (91.5%) (Figure S1; Table S3).

2.3 | Virus-Induced Gene Silencing of CASs

Five putative CASs were previously identified in pot marigold but had not been functionally characterized (Golubova et al. 2025). The protein sequences of these putative CASs (CoCAS1, 2, 3, 4, and 5) were used as a queries in tBLASTn to search genomes of *Helianthus anuus* (Ha), *A. thaliana* (At), *Nicotiana benthamiana* (Nb), *C. cardunculus* var. scolymus (Cc), *A. annua* (Aa), *L. sativa* (Ls), *C. endivia* (Ce), and *Amborella trichopoda* (Amt). Protein sequences with at least 87% coverage and 65.7% identity were selected as candidate CASs, aligned and used to contrast a maximum likelihood phylogenetic tree (Figure 3A). The relative gene expression of the *CoCAS* orthologues across leaf and floral tissues was analyzed as described above and *CoCAS2* and *4* were found to be highly expressed in leaves and selected as targets for VIGS (Figure 3B). To construct VIGS vectors for *CoCAS2* and *4*, a 300 bp region in which sequence identity of these two genes is 100% was identified. This region was amplified and cloned into pTRV2 fused to *CoPDS* (Figure 3C and Table S1). Subsequently, plants were co-infiltrated with pTRV1 and either the control plasmid (pTRV2-PDS:GFP) or the experimental plasmid (pTRV2-PDS:CAS).

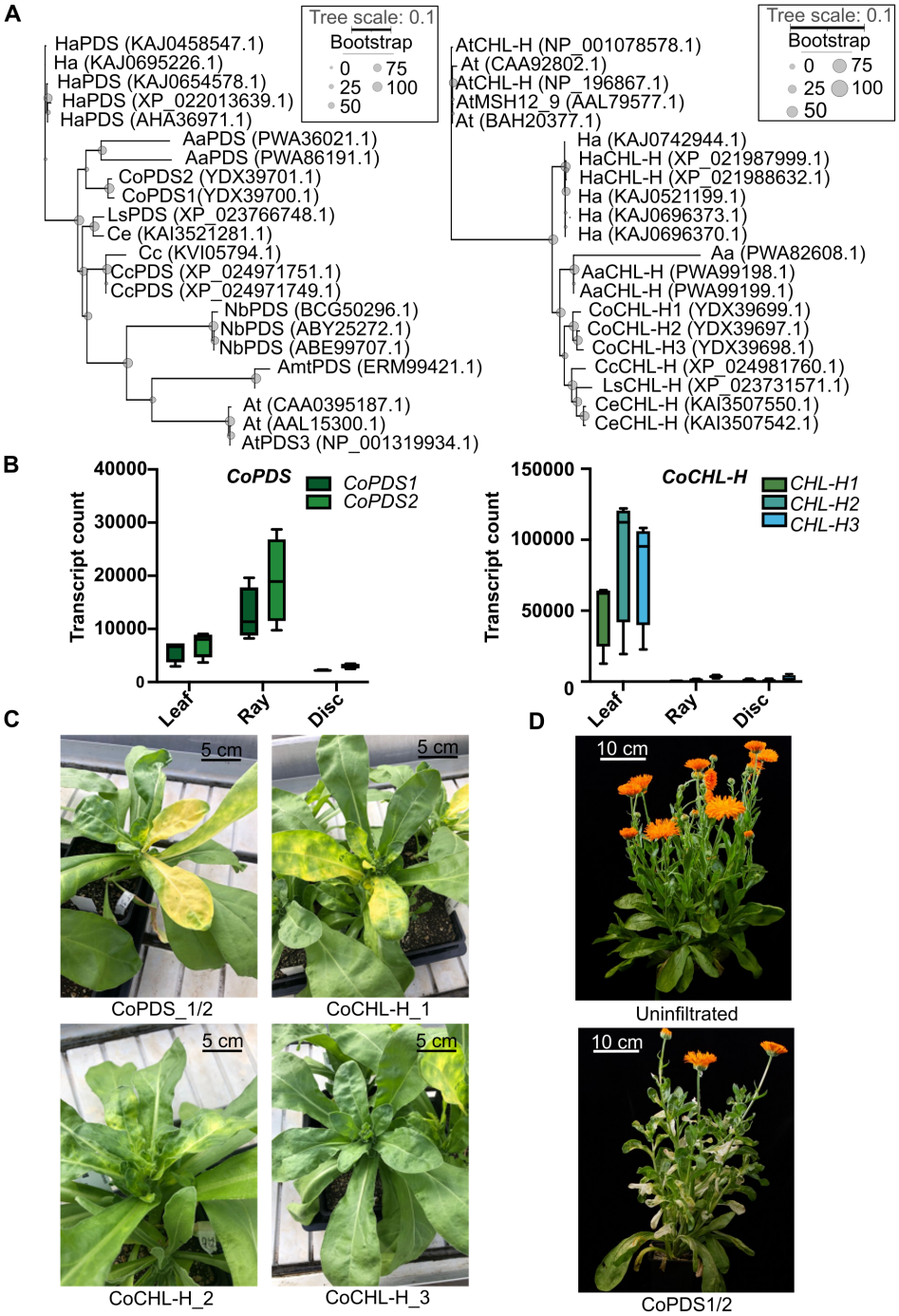


FIGURE 2 | **Virus-induced gene silencing of phytoene desaturase (PDS) and *magnesium chelatase subunit H* (*CHL-H*) *in Calendula officinalis* (pot marigold).** (A) Maximum likelihood phylogeny of PDS and CHL-H protein sequences. *Helianthus anuus* (Ha), *Arabidopsis thaliana* (At), *Nicotiana benthamiana* (Nb), *Cynara cardunculus* var. scolymus (Cc), *Artemisia annua* (Aa), *Lactuca sativa* (Ls), *Cichorium endivia* (Ce), and *Amborella trichopoda* (Amt). The scale bar indicates the number of substitutions. *CoPDS* and *CoCHL* genes are named according to a previously published transcriptome (https://doi.org/10.5281/zenodo.13869958). (B) Expression of candidate *CoPDS* and *CoCHL* genes in *C. officinalis* leaf, ray floret, and disc floret tissues. Boxplots show normalized transcript counts of four biological replicates; the center line denotes the median value; the boxes show the 25th to 75th percentiles and the whiskers mark the minimum and maximum values. (C) Images of representative plants infiltrated with VIGS vectors targeting *CoPDS* and *CoCHL*14 days after infiltration. Scale bar = 5 cm. (D) Images of control plant and representative plant infiltrated with VIGS vectors 35 days after infiltration. Scale bar = 10 cm.

2.4 | Reduced Expression of Pot Marigold CASs Alters Sterol Accumulation

The first committed step of phytosterol biosynthesis is the conversion of 2,3-oxidosqualene to cycloartenol by CASs. This is then converted to campestrol (used to produce brassinolides), or to stigmasterol via isofucosterol and β-sitosterol, which are all integral membrane components (Figure 4A). First, the expression levels of the target genes were analyzed. Samples were taken from leaves that showed a bleaching phenotype

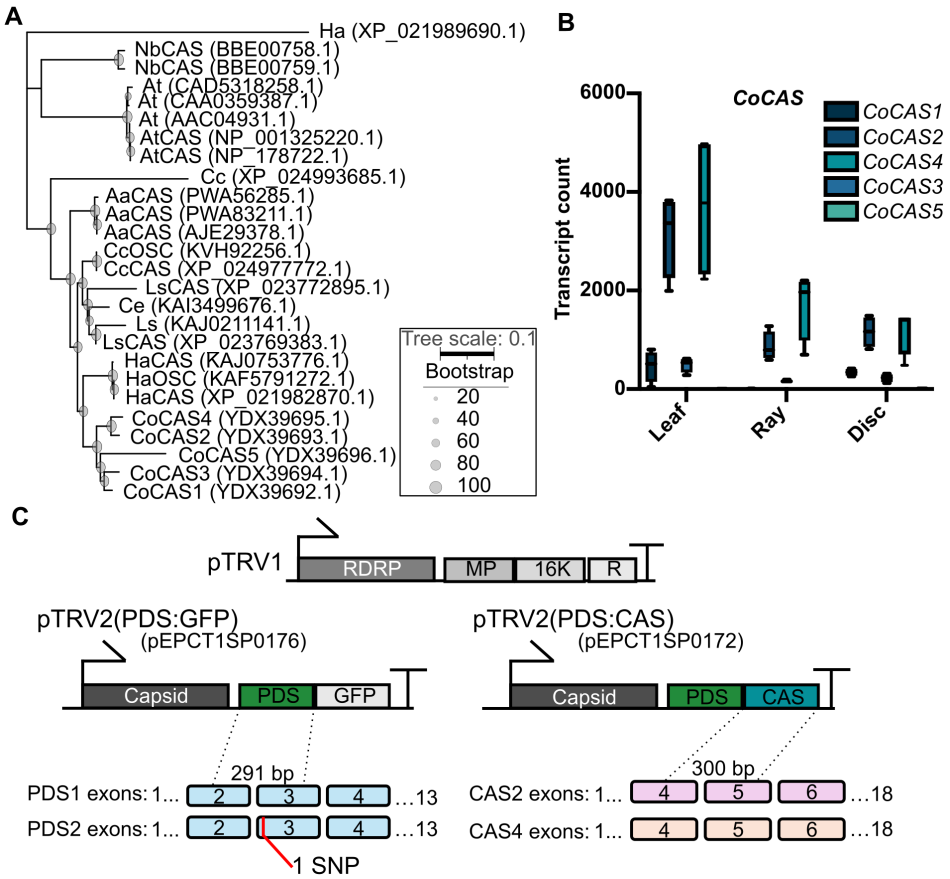


FIGURE 3 | **Identification of candidate Calendula officinalis (pot marigold) cycloartenol synthase (CAS) genes.** (A) Maximum likelihood phylogeny of CASs. Scale bar indicates the number of substitutions. *Helianthus anuus* (Ha), *Arabidopsis thaliana* (At), *Nicotiana benthamiana* (Nb), *Cynara cardunculus* var. scolymus (Cc), *Artemisia annua* (Aa), *Lactuca sativa* (Ls) and *Cichorium endivia* (Ce), and *Amborella trichopoda* (Amt). CoCAS 1–5 were identified in Golubova et al. 2025. (B) Expression of candidate CoCAS genes in *C. officinalis* leaf, ray floret and disc floret tissues. Boxplots show normalized transcript counts of four biological replicates; the center line denotes the median value; the boxes show the 25th to 75th percentiles and the whiskers mark the minimum and maximum values. (C) Schematics of plasmids for virus-induced gene silencing. A fragment of the visual marker gene CoPDS1/2 is fused to a fragment of either a control (GFP) or target gene (CAS).

38 days after infiltration. RNA was extracted and gene expression analyzed by qRT-PCR. The expression levels of CoCAS2 and CoCAS4 were significantly reduced (69.0% and 70.5% respectively) in plants infiltrated with pTRV1 + pTRV-PDS:CAS compared to the control (Figure 4B and Table S4). Samples from the same leaves were extracted in ethyl acetate, dried and derivatized with *N*-methyl-*N*-(trimethylsilyl)trifluoroacetamide and analyzed by gas chromatography–mass spectrometry (GC–MS). Peaks were identified by comparison to authentic standards (Figure S2). Levels of campesterol and β-sitosterol were comparable between those infiltrated with the control plasmid (pTRV2-PDS:GFP) and those targeting CoCAS2 and 4 (pTRV2-PDS:CAS) (Figure 4C and Table S4). However, the accumulation of stigmasterol was reduced in plants in which CoCAS2 and 4 expression was reduced and the accumulation of isofucosterol was increased (Figure 4C and Table S4). To confirm that silencing of CoPDS1/2 did not affect sterol accumulation, sterol levels were also compared to uninfiltrated plants, and no significant differences were observed (Figure S3 and Table S5).

Finally, to assess if VIGS can be used to study florally expressed genes, samples of ray floret tissues were collected from the flowers of plants infiltrated with the same constructs 38 days after infiltration. In addition, a second set of plasmid vectors was constructed in which a fragment of FLOWERING LOCUS T, previously reported to facilitate transport of infiltrated small RNAs to floral meristems (Ellison et al. 2020), was fused to the 3′ end of the *PDS* and *CAS* gene fragments (Table S1). However, no reduction in the expression of the target genes was identified in the flowers using either set of vectors (Figure S4 and Table S6).

3 | Discussion

VIGS is a powerful method for functional characterization of endogenous plant genes. To establish a VIGS method for pot marigold, we first investigated agroinfiltration, finding that *Agrobacterium tumefaciens* AGL1 and LBA4404 gave the highest levels of expression (Figure 1). *A. tumefaciens* AGL1 has a similar chromosomal background to the wild-type strain, C58, containing a 2.8 Mb circular chromosome and a 2 Mb linear chromosome (De Saeger et al. 2021). It also contains the pTiBo542 tumor-inducing (Ti) plasmid, sometimes called a hypervirulence plasmid due to the presence of additional

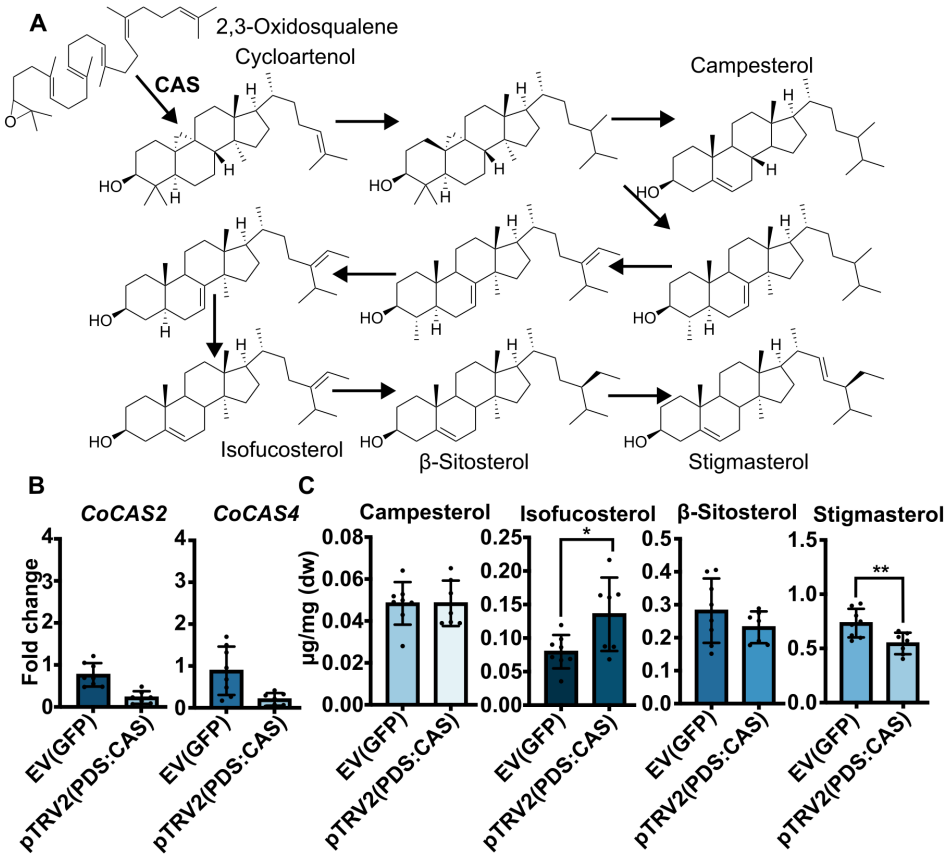


FIGURE 4 | **Virus-induced gene silencing of cycloartenol synthases reduced the accumulation of stigmasterol.** (A) Schematic of the conversion of 2,3-oxidosqualene to cycloartenol by CAS and subsequent modifications to campesterol, isofucosterol, β-sitosterol, and stigmasterol. (B) Expression levels of *CoCAS* genes in pot marigold leaves 38 days after infiltration with VIGS vectors as determined by qRT-PCR; $n \geq 7$. Bars show the mean and standard error of four replicates. Statistical significance was determined for *CoCAS2* using a Student's *t*-test. For *CoCAS4*, a Mann–Whitney *U* test was used as there was no evidence of equal variance or normal distribution (Table S4). (C) Quantification of stigmasterol, isofucosterol, β-sitosterol, and campesterol in plants in which expression of *CoCAS* was reduced by VIGS. Metabolites were quantified by GC–MS using an internal standard. $n \geq 7$; statistical significance was calculated using a Student's *t*-test (Table S4). EV = empty vector (pTRV2-PDS:GFP); CAS = pTRV2-PDS:CAS.

copies of the *virulence* (*vir*) genes, and a 0.54 Mb pAtC58 accessory plasmid. Transformation efficiency has been shown to increase with *A. tumefaciens* strains containing pTiBo542 (Komari 1990). Furthermore, AGL1 carries an insertion mutation in its *recA* general recombination gene (Lazo et al. 1991), which may also impact plasmid integrity and therefore efficiency of transformation. *A. tumefaciens* LBA4404 has an Ach5 chromosomal background, which is also similar to C58, (De Saeger et al. 2021). Both AGL1 and LBA4404 are widely used and have been shown to transform numerous plant species (Lee and Gelvin 2008).

In this study, VIGS was achieved by injecting *A. tumefaciens* into the midrib vein of immature (nonflowering) pot marigold plants (Figure 4 and Data S1). The use of *PDS1* as a marker gene enabled viral spread to be tracked, guiding the sampling of tissues (Figures 1 and 4). This was important as silencing only occurred in some sectors of some leaves. Alternative viral vectors may improve infection, as might different methods for delivery of *A. tumefaciens*. Previously, vacuum infiltration of seeds improved VIGS efficiency in sunflowers. In *Nepeta* sp. (catmint), *A. tumefaciens* dropped onto wounds enabled VIGS, and in sweet wormwood, the use of the surfactants Silwet L-77 and Silwet S-408 improved the efficiency of *A. tumefaciens*-mediated transient gene expression (Elfahmi et al. 2014; Palmer and O'Connor 2020; Mardini et al. 2024).

Several secondary metabolites are known to be controlled via feedback mechanisms (Li, Grotewold, and Dudareva 2024). VIGS of *CoCAS2* and *CoCAS4* resulted in less stigmasterol but not of campesterol, isofucosterol, or β-sitosterol (2024). Although more detailed investigations are required, this suggests mechanisms exist to maintain some membrane components and flux to brassinolides, possibly by feedback at the protein or the transcriptional level. Silencing of *CAS* genes has been observed to have different effects in other species: In tomato, silencing of *SlCAS* reduced the accumulation of cholesterol, stigmasterol, *β*-sitosterol, isofucosterol, and cycloartenol, revealing that SlCAS catalyzes the production of a common precursor for tomato cholesterol and phytosterol metabolism (Sonawane et al. 2016). In *N. benthamiana*, silencing *NbCAS1* increased the expression of *NbHMGR1*, which acts further up in the mevalonate pathway converting 3-hydroxy-3-methyl-3-glutaryl coenzyme A to mevalonate, which is used to produce the 2,3-oxidosqualene precursor for sterol production. In contrast, the expression of *NbSSR2* and

NbSMT1, which encode enzymes involved in the production of steroidal glycoalkaloids and sterols, respectively, was reduced (Atsumi et al. 2018). These studies demonstrate that VIGS can be combined with quantification of transcripts and metabolites to investigate the regulation of metabolic pathways. In the future, comparative studies may reveal commonalities and divergences in sterol metabolism between plant lineages. Demonstrating efficient VIGS methods for new species contributes to this aim.

There are few reports of VIGS in floral tissues, though TRV-based vectors have been used to study flower floral senescence in *Petunia hybrida* (Chen et al. 2004). TRV is known to systemically infect this and other solanaceae species. VIGS of floral tissues was also demonstrated in *Rosa chinensis* (China rose) and used to study anthocyanin biosynthesis (Yan et al. 2020). In Asteraceae, VIGS and overexpression constructs were infiltrated into the detached petals of *Gerbera hybrida* (Jiang et al. 2022), but entry of viruses into floral meristems is limited (Li, Hong, et al. 2024). Some plant mRNAs are mobile and can move between cells or organs to transmit environmental signals into developmental programs (Luo et al. 2024). For example, the mRNA of *FLOWERING TIME* (*FT*), which encodes for a mobile protein that mediates the onset of flowering, was itself shown to move from leaves to the shoot apical meristem (SAM) through the phloem (Pin and Nilsson 2012; Liu et al. 2013). In 2020, Ellison et al. reported that TRV vectors expressing single guide RNAs (sgRNA) could be used to produce heritable mutations following transient expression in the leaves of *N. benthamina* plants constitutively expressing Cas9 (Ellison et al. 2020). They reported that the addition of a *FT* tag to sgRNAs increased the frequency of heritable edits by promoting entry into the shoot apical meristem, which has been successfully employed to edit targeted in several studies including our own (Dudley et al. 2022; Vollheyde et al. 2023). In this study, we fused an identical *FT* tag to target RNAs in VIGS constructs. However, this did not enable gene silencing in floral tissues of pot marigold. The identification of alternative VIGS vectors with systemic infection may improve VIGS in floral tissues of Asteraceae.

4 | Methods

4.1 | Plant Growth

Seeds of *C. officinalis* (pot marigold) were purchased from Chiltern Seeds (Wallingford, UK). Seeds were sown in 9-cm plastic pots with Levington F2 starter (100% peat). Approximately 10 days after emergence, seedlings were transplanted into 11-cm plastic pots containing 60% peat, 20% grit, 20% perlite, 2.25 kg/m^3 dolomitic limestone, 1.3 kg/m^3 PG mix, and 3 kg/m^3 osmocote exact. All plants were grown in summer glasshouse conditions with natural day length and temperature. *N. benthamiana* was sewn in a 10-cm plastic pot and cultivated in a peat-based potting mix (90% peat, 10% grit, with 4 kg/m^3 dolomitic limestone, 0.75 kg/m^3 powdered compound fertilizer, 1.5 kg/m^3 slow-release fertilizer). *N. benthamiana* plants were grown in a controlled environment room with 16 h light, 8 h dark at 22°C, 80% humidity, and ~200 μmol/m^2/s light intensity for 28 days prior to infiltration.

4.2 | Transformation of *A. tumefaciens*

Aliquots of 40 μL electrocompetent *A. tumefaciens* were incubated on ice with 200 ng of plasmid DNA for 2 min. Electroporation was performed in ice-chilled 2-mm electroporation cuvettes (Geneflow) using a MicroPulser Electroporator (Bio-Rad) at 2.2 kV with < 1 s pulse duration. Immediately after electroporation, 400 μL of LB were added and cells were transferred to 2-mL microcentrifuge tubes and incubated at 28°C for 2–3 h at 200 rpm. Twenty microliters was plated onto LB-agar with appropriate antibiotics, using 6-mm glass beads. Plates were dried for 5 min and incubated upside down at 28°C for 48 h.

4.3 | Transient Expression of Luciferase

A. tumefaciens strains AGL1, LBA4404, and GV3101 harboring the firefly luciferase (LucF) under the control of the Cauliflower Mosaic Virus 35 s promoter (CaMVp) (pEPCTαKN0001; Addgene #187568) were grown in LB medium supplemented with 50 μg/mL kanamycin plus ether 100 μg/mL rifampicin and 50 μg/m carbenicillin (AGL1); 100 μg/mL rifampicin and 50 μg/m streptomycin (LBA4404) or 100 μg/mL rifampicin and 20 μg/mL gentamicin (GV3101), respectively, for each *A. tumefaciens* strain. Details of all plasmid vectors are provided in Table S1 and details of *A. tumefaciens* strains are provided in Table S7. Cultures were incubated for 16 h at 28°C/220 rpm. Overnight saturated cultures were centrifuged at 3000 *g* for 20 min at room temperature, and cells were resuspended in infiltration medium (10 mM 2-[N-morpholino]ethanesulfonic acid [MES] pH 5.6, 10 mM MgCl2, 200 μM 3′,5′-dimethoxy-4′-hydroxyacetophenone [acetosyringone]) to OD600 0.8, and incubated at room temperature for 2–3 h. *A. tumefaciens* cultures were infiltrated into the abaxial side of leaves of 28-day-old nonflowering *N. benthamiana* and pot marigold plants with three to four fully expanded true leaves using a 1 mL needleless syringe. Plants were grown in controlled environment chambers (16 h light, 8 h dark; 22°C; 120–180 μmol/m^2/s light intensity). After 5 days, two 1-cm diameter discs were sampled from infiltrated leaves. Luciferase expression was detected using the Luciferase reporter assay system (Promega, Madison, WI, USA). Leaf tissue was homogenized in 180 μL passive lysis buffer (Promega) with protease inhibitor (P9599, Sigma-Aldrich, Dorset, UK). Following incubation on ice for 15 min and centrifugation (14,000 *g*; 2 min; 4°C), 10 μL of supernatant was diluted 1:10 in passive lysis buffer. Ten microliters of this dilution was further diluted 1:3 in passive lysis buffer and an equal volume (30 μL) of ONE-Glo EX Luciferase Assay Reagent (Promega) was added. After 10 min at room temperature, luminescence was quantified using a GloMax 96 Microplate Luminometer (Promega) with a 10-s read time and 1-s settling time.

4.4 | Identification of Candidate Genes and Phylogenetic Analysis

Candidate *CoPDS* and *CoCHL-H* genes were identified using tBLASTn to search the pot marigold genome using NbPDS (LC543532.1) and NtCHL-H (NM_001325713.1) as queries. The

identification of *CoCAS* was previously described (Golubova et al. 2025). The translated protein sequences of the retrieved pot marigold genes were used to search the publicly available translatomes of *A. trichopoda* (txid:13333), *A. thaliana* (txid:3702), *N. benthamiana* (txid:4100), *A. annua* (txid:35608), *L.sativa* (txid:4236), *C. endive* (txid:114280), *Taraxacum kok-saghyz* (txid:333970), *H.anuus* (txid:4232), *C.seticuspe* (txid:1111766), and *Cynara cardunculus* (txid:4265). Sequences with 87% coverage and 65.7% identity to CoCAS, 77% coverage and protein identity to CoCHL-H and 91% coverage and 81.7% identity to CoPDS candidates were selected. Protein sequences were aligned using MAFFT (v7.511) and trimmed using ClipKIT with smartgap mode (v2.1.3). Maximum likelihood trees were inferred using IQ-TREE and models were selected using ModelFinder (CAS = JTTDCMut+G4, CHL-H=VT+G4, PDS = JTT+i+G4) (Kalyaanamoorthy et al. 2017). Differential expression analysis was performed as previously described using existing data (https://doi.org/10.5281/zenodo.13869958) (Golubova et al. 2025). The coding sequences of *C. officinalis* genes are available at the following accession numbers: *CoCAS1* (PZ276377), *CoCAS2* (PZ276378), *CoCAS3* (PZ276379), *CoCAS4* (PZ276380), *CoCAS5* (PZ276381), *CoCHL-H1* (PZ276384), *CoCHL-H2* (PZ276382), *CoCHL-H3* (PZ276383), *CoPDS1* (PZ276385), *CoPDS2* (PZ276386), *CoSAND* (PZ276387), and *CoPP2A* (PZ276388).

4.5 | Construction of Plasmid Vectors for Virus-Induced Gene Silencing

Target sequences were amplified from cDNA or existing plasmids using primers with extension that enabled cloning into BsaI sites of pTRV2 (Addgene #105349). Primer sequences are provided in Table S8. Constructs were assembled using a one-step digestion-ligation reaction as previously described (Cai et al. 2020). Sequence-verified constructs were transformed into *A. tumefaciens* AGL1 by electroporation. The details of all plasmid vectors are provided in Table S1.

4.6 | *Agrobacterium* Infiltration for VIGS

Cultures of electrocompetent *A. tumefaciens* AGL1 with pTRV1 (pNJB069) or pTRV2 (Addgene #105349) were grown as described above. Cells were collected by centrifugation and resuspended in infiltration medium with acetosyringone to OD_{600} 0.8. Cultures with pTRV1 and pTRV2 were in a 1:1 ratio prior to infiltration. For *N. benthamiana*, 28 days old plants were infiltrated as described above. The first true leaves of 28-day-old pot marigold plants were infiltrated as described above or by using a 1-mL syringe with a needle to inject cultures into the midrib until liquid was observed to spread through the plant (Data S1).

4.7 | Purification of Nucleic Acids

Two samples of total RNA were purified from leaf and ray floret tissue collected from four independent plants per construct, snap-frozen in liquid nitrogen and stored at −70°C. RNA was extracted using the Spectrum Plant Total RNA Kit (STRN250; Merck, Darmstadt, Germany) following the manufacturer's instructions except that during column washing, 300 μL of column wash 1 was used to wash RNA and then 80 μL of DNase I (RNA-Free Dnase Set 79254; Qiagen, Hilden, Germany) was added to the column and incubated for 15 min followed by 500 μL of wash 1. RNA integrity was assessed by electrophoresis on a 1.5% agarose gel and using a Bioanalyzer (Agilent Technologies, Sata Clara, CA, USA).

4.8 | Quantitative Reverse Transcription PCR

Reverse transcription was performed using M-MLV cDNA (Sigma: M1302) according to the manufacturer's instructions. Following first strand synthesis, reactions were inactivated at 70°C for 15 min and cDNA was diluted 1:10 in TE (5 mM Tris–HCl + 0.5 mM EDTA, pH 8.0). As previously reported, SAND and PP2A were used as reference genes (Golubova et al. 2025). Amplification was performed in 10 μL reactions (0.2 μM each primer, 6 ng cDNA, 1 μL SYBR Green Jumpstart Taq ReadyMix) and incubated at 94°C for 2 min and 40× (94°C for 15 s and 58°C for 60 s). Two qPCR reactions (technical replicates) were performed for each of four biological samples (independently infiltrated plants). Control reactions (no reverse transcriptase; no template controls) had Cq values of > 35. Relative expression analysis was calculated using the ΔΔCt method (Livak and Schmittgen 2001).

4.9 | Metabolite Extraction and GC–MS Analysis

Metabolites were extracted from 30 mg of freeze-dried plant material by homogenization with samples mixed in 500 μL ethyl acetate (Sigma Aldrich, Burlington, MA, USA) at 700 rpm at 40°C for 2 h, incubated at room temperature for 48 h. Following centrifugation at 21,130 x *g* for 5 min, 50 μL of supernatant was transferred to a 2-mL glass vial and dried in a centrifugal evaporator. Samples were derivatized with 50 μL *N*-Methyl-*N*-(trimethylsilyl)trifluoroacetamide (Sigma Aldrich) at 37°C for 30 min and transferred to glass inserts in 2-mL glass vials for GC–MS analysis on a 7890B GC (Agilent; Santa Clara, CA, USA) with a Zebron ZB5-HT Inferno column (Phenomenex; Washington, DC, USA) as previously described (Golubova et al. 2025). Data analysis was carried out using MassHunter workstation software (Agilent).

4.10 | Statistics and Reproducibility

Analyses including metabolomics, transcriptomics and gene expression via qPCR were performed with a minimum of 6 biological replicates. Outliers were identified using a Grubbs, which was used to exclude two replicates from uninfiltrated plants and a single replicate from pTRV2(PDS:CAS) (Table S9). The investigators were not blinded during experiments or analysis. Exact *p* values and test statistics are provided in Tables S2–S6 alongside tested assumptions for each statistical test.

Author Contributions

C.T., D.C., and N.P. conceptualized the study. D.C. performed luciferase assays. M.S., D.C., and C.T. identified candidate genes and performed phylogenetic analyses. M.S., D.C., and C.T. extracted RNA. D.C. and C.T. cloned pTRV plasmids. C.T. and D.C. performed qRT-PCR. C.T.

performed metabolic profiling. M.S., C.T., and N.P. were responsible for supervision and project management. N.P. was responsible for fundraising. D.C., C.T., and N.P. drafted the figures and text. All authors contributed to revisions and editing.

Acknowledgments

Plasmids pNJB069 (TRV1) were a gift from Daniel Voytas, and pTRV2 (Addgene #105349) was a gift from Johannes Stuttmann. We also thank the John Innes Centre horticultural services team for assistance with plant husbandry and the John Innes Centre metabolomics facility for assistance with GC–MS. Thanks to Sasha Stanbridge from the Earlham Institute for assistance with photography of *C. officinalis* plants. Reference standards: β-sitosterol, stigmasterol and campesterol were kindly provided by Anne Osbourn, John Innes Centre, Norwich, UK.

Funding

We gratefully acknowledge the support of the Biotechnology and Biological Sciences Research Council (BBSRC), part of UK Research and Innovation for funding via Grant BB/W014173/1 and the Earlham Institute Strategic Programme grant, Decoding Biodiversity (BBX011089/1) and its constituent work package (BBS/E/ER/230002B). D.C. is supported by a scholarship from the John Innes Foundation.

Conflicts of Interest

The authors declare no conflicts of interest.

Data Availability Statement

The data that supports the findings of this study are available in the supplementary material of this article.

References

Alam, P., A. Mohammad, M. M. Ahmad, et al. 2014. "Efficient Method for *Agrobacterium* Mediated Transformation of Artemisia annua L." *Recent Patents on Biotechnology* 8: 102–107.

Atsumi, G., U. Kagaya, N. Tabayashi, and T. Matsumura. 2018. "Analysis of the Mechanisms Regulating the Expression of Isoprenoid Biosynthesis Genes in Hydroponically-Grown *Nicotiana benthamiana* Plants Using Virus-Induced Gene Silencing." *Scientific Reports* 8: 14804.

Babiychuk, E., P. Bouvier-Navé, V. Compagnon, et al. 2008. "Allelic Mutant Series Reveal Distinct Functions for Arabidopsis Cycloartenol Synthase 1 in Cell Viability and Plastid Biogenesis." *Proceedings of the National Academy of Sciences of the United States of America* 105: 3163–3168.

Broderick, S. R., and M. L. Jones. 2014. "An Optimized Protocol to Increase Virus-Induced Gene Silencing Efficiency and Minimize Viral Symptoms in Petunia." *Plant Molecular Biology Reporter* 32: 219–233.

Burch-Smith, T. M., M. Schiff, Y. Liu, and S. P. Dinesh-Kumar. 2006. "Efficient Virus-Induced Gene Silencing in Arabidopsis." *Plant Physiology* 142: 21–27.

Cai, Y.-M., J. A. Carrasco Lopez, and N. J. Patron. 2020. "Phytobricks: Manual and Automated Assembly of Constructs for Engineering Plants." In *DNA Cloning and Assembly: Methods and Protocols*, edited by S. Chandran and K. W. George, 179–199. Springer US.

Chen, J.-C., C.-Z. Jiang, T. E. Gookin, D. A. Hunter, D. G. Clark, and M. S. Reid. 2004. "Chalcone Synthase as a Reporter in Virus-Induced Gene Silencing Studies of Flower Senescence." *Plant Molecular Biology* 55: 521–530.

Darqui, F. S., L. M. Radonic, V. C. Beracochea, H. E. Hopp, and M. López Bilbao. 2021. "Peculiarities of the Transformation of Family Species: The Cases of Sunflower and Lettuce." *Frontiers in Plant Science* 12: 767459.

De Saeger, J., J. Park, H. S. Chung, et al. 2021. "*Agrobacterium* Strains and Strain Improvement: Present and Outlook." *Biotechnology Advances* 53: 107677.

Deng, X., P. Elomaa, C. X. Nguyen, T. Hytönen, J. P. T. Valkonen, and T. H. Teeri. 2012. "Virus-Induced Gene Silencing for Asteraceae—A Reverse Genetics Approach for Functional Genomics in *Gerbera hybrida*." *Plant Biotechnology Journal* 10: 970–978.

Ding, X. S., C. S. Rao, and R. S. Nelson. 2007. "Analysis of Gene Function in Rice Through Virus-Induced Gene Silencing." *Methods in Molecular Biology* 354: 145–160.

Długosz, M., M. Markowski, and C. Pączkowski. 2018. "Source of Nitrogen as a Factor Limiting Saponin Production by Hairy Root and Suspension Cultures of *Calendula officinalis* L." *Acta Physiologiae Plantarum* 40: 1–14.

Dommes, A. B., T. Gross, D. B. Herbert, K. I. Kivivirta, and A. Becker. 2019. "Virus-Induced Gene Silencing: Empowering Genetics in Non-Model Organisms." *Journal of Experimental Botany* 70: 757–770.

Dudley, Q. M., S. Jo, D. A. S. Guerrero, et al. 2022. "Reconstitution of Monoterpene Indole Alkaloid Biosynthesis in Genome Engineered *Nicotiana benthamiana*." *Communications Biology* 5: 949.

Elfahmi, S. Suhandono, and A. Chahyadi. 2014. "Optimization of Genetic Transformation of *Artemisia annua* L. Using *Agrobacterium* for Artemisinin Production." *Pharmacognosy Magazine* 10: S176–S180.

Ellison, E. E., U. Nagalakshmi, M. E. Gamo, P.-J. Huang, S. Dinesh-Kumar, and D. F. Voytas. 2020. "Multiplexed Heritable Gene Editing Using RNA Viruses and Mobile Single Guide RNAs." *Nature Plants* 6: 620–624.

Golubova, D., M. Salmon, H. Su, et al. 2025. "Biosynthesis and Bioactivity of Anti-Inflammatory Triterpenoids in *Calendula officinalis*." *Nature Communications* 16: 6941.

Hassani, D., A. Taheri, X. Fu, et al. 2023. "Elevation of Artemisinin Content by Co-Transformation of Artemisinin Biosynthetic Pathway Genes and Trichome-Specific Transcription Factors in." *Frontiers in Plant Science* 14: 1118082.

Hein, I., M. Barciszewska-Pacak, K. Hrubikova, et al. 2005. "Virus-Induced Gene Silencing-Based Functional Characterization of Genes Associated With Powdery Mildew Resistance in Barley." *Plant Physiology* 138: 2155–2164.

Hiriart, J.-B., E.-M. Aro, and K. Lehto. 2003. "Dynamics of the VIGS-Mediated Chimeric Silencing of the *Nicotiana benthamiana* ChlH Gene and of the Tobacco Mosaic Virus Vector." *Molecular Plant-Microbe Interactions* 16: 99–106.

Jiang, R., W. Yuan, W. Yao, X. Jin, X. Wang, and Y. Wang. 2022. "A Regulatory GhBPE-GhPRGL Module Maintains Ray Petal Length in *Gerbera hybrida*." *Molecular Horticulture* 2: 9.

Kalyaanamoorthy, S., B. Q. Minh, T. K. F. Wong, A. von Haeseler, and L. S. Jermiin. 2017. "ModelFinder: Fast Model Selection for Accurate Phylogenetic Estimates." *Nature Methods* 14: 587–589.

Komari, T. 1990. "Transformation of Cultured Cells of *Chenopodium quinoa* by Binary Vectors That Carry a Fragment of DNA From the Virulence Region of pTiBo542." *Plant Cell Reports* 9: 303–306.

Kumagai, M. H., J. Donson, G. della-Cioppa, D. Harvey, K. Hanley, and L. K. Grill. 1995. "Cytoplasmic Inhibition of Carotenoid Biosynthesis With Virus-Derived RNA." *Proceedings of the National Academy of Sciences of the United States of America* 92: 1679–1683.

Lazo, G. R., P. A. Stein, and R. A. Ludwig. 1991. "A DNA Transformation-Competent Arabidopsis Genomic Library in Agrobacterium." *Biotechnology (N Y)* 9: 963–967.

Lee, L.-Y., and S. B. Gelvin. 2008. "T-DNA Binary Vectors and Systems." *Plant Physiology* 146: 325–332.

Li, J., E. Hong, P. Zhang, et al. 2024. "Antiviral Defense in Plant Stem Cells." *Trends in Plant Science* 9: 955–957.

Li, Y., E. Grotewold, and N. Dudareva. 2024. "Enough Is Enough: Feedback Control of Specialized Metabolism." *Trends in Plant Science* 29: 514–523.

Liscombe, D. K., and S. E. O'Connor. 2011. "A Virus-Induced Gene Silencing Approach to Understanding Alkaloid Metabolism in *Catharanthus roseus*." *Phytochemistry* 72: 1969–1977.

Liu, L., Y. Zhu, L. Shen, and H. Yu. 2013. "Emerging Insights Into Florigen Transport." *Current Opinion in Plant Biology* 16: 607–613.

Liu, Y., R. Lyu, J. J. Singleton, B. Patra, S. Pattanaik, and L. Yuan. 2024. "A Cotyledon-Based Virus-Induced Gene Silencing (Cotyledon-VIGS) Approach to Study Specialized Metabolism in Medicinal Plants." *Plant Methods* 20: 26.

Livak, K. J., and T. D. Schmittgen. 2001. "Analysis of Relative Gene Expression Data Using Real-Time Quantitative PCR and the 2(-Delta Delta C(T)) Method." *Methods (San Diego, Calif.)* 25: 402–408.

Lopez-Gomollon, S., and D. C. Baulcombe. 2022. "Roles of RNA Silencing in Viral and Non-Viral Plant Immunity and in the Crosstalk Between Disease Resistance Systems." *Nature Reviews. Molecular Cell Biology* 23: 645–662.

Luo, K.-R., N.-C. Huang, Y.-H. Chang, Y.-W. Jan, and T.-S. Yu. 2024. "Arabidopsis Cyclophilins Direct Intracellular Transport of Mobile mRNA via Organelle Hitchhiking." *Nature Plants* 10: 161–171.

Mardini, M., M. Kazancev, E. Ivoilova, et al. 2024. "Advancing Virus-Induced Gene Silencing in Sunflower: Key Factors of VIGS Spreading and a Novel Simple Protocol." *Plant Methods* 20: 122.

Matvieieva, N., T. Bohdanovych, V. Belokurova, et al. 2025. "Variability in Growth and Biosynthetic Activity of Hairy Roots." *Preparative Biochemistry & Biotechnology* 55: 381–391.

Misra, R. C., S. Sharma, A. Garg, and S. Ghosh. 2020. "Virus-Induced Gene Silencing in Sweet Basil (*Ocimum basilicum*)." *Methods in Molecular Biology* 2172: 123–138.

Moglia, A., A. Acquadro, K. Eljounaidi, et al. 2016. "Genome-Wide Identification of BAHD Acyltransferases and Characterization of HQT-Like Enzymes Involved in Caffeoylquinic Acid Synthesis in Globe Artichoke." *Frontiers in Plant Science* 7: 1424.

Müller, A., M. Iser, and D. Hess. 2001. "Stable Transformation of Sunflower (Helianthus annuus L.) Using a Non-Meristematic Regeneration Protocol and Green Fluorescent Protein as a Vital Marker." *Transgenic Research* 10: 435–444.

Navarro Gallón, S. M., C. Elejalde-Palmett, D. Daudu, et al. 2017. "Virus-Induced Gene Silencing of the Two Squalene Synthase Isoforms of Apple Tree (*Malus* × domestica L.) Negatively Impacts Phytosterol Biosynthesis, Plastid Pigmentation and Leaf Growth." *Planta* 246: 45–60.

Ni, J., S. Wang, W. Yu, et al. 2023. "The Ethylene-Responsive Transcription Factor PpERF9 Represses PpRAP2.4 and PpMYB114 via Histone Deacetylation To Inhibit Anthocyanin Biosynthesis in Pear." *Plant Cell* 35, no. 6: 2271–2292. https://doi.org/10.1093/plcell/koad077.

Palmer, L., and S. E. O'Connor. 2020. "Virus-Induced Genee Silencing in Nepeta." *Methods in Molecular Biology* 2172: 111–121.

Pin, P. A., and O. Nilsson. 2012. "The Multifaceted Roles of Flowering Locus T in Plant Development." *Plant, Cell & Environment* 35: 1742–1755.

Ratcliff, F., A. M. Martin-Hernandez, and D. C. Baulcombe. 2001. "Technical Advance. Tobacco Rattle Virus as a Vector for Analysis of Gene Function by Silencing." *Plant Journal* 25: 237–245.

Roche, M. C., W. Liu, and R. Hernández. 2025. "An Improved Method for *Agrobacterium*-Mediated Genetic Transformation of Three Types of Lettuce." *Plants* 14, no. 4: 620.

Sonawane, P. D., J. Pollier, S. Panda, et al. 2016. "Plant Cholesterol Biosynthetic Pathway Overlaps With Phytosterol Metabolism." *Nature Plants* 3: 16205.

Tian, Y., Y. Fang, K. Zhang, et al. 2024. "Applications of Virus-Induced Gene Silencing in Cotton." *Plants* 13, no. 2: 272.

Vollheyde, K., Q. M. Dudley, T. Yang, et al. 2023. "An Improved *Nicotiana benthamiana* Bioproduction Chassis Provides Novel Insights Into Nicotine Biosynthesis." *New Phytologist* 240: 302–317.

Wang, L., Y. Wu, W. Du, et al. 2021. "Virus-Induced Gene Silencing (VIGS) Analysis Shows Involvement of the LsSTPK Gene in Lettuce (L.) in High Temperature-Induced Bolting." *Plant Signaling & Behavior* 16: 1913845.

Wang, R., X. Yang, N. Wang, et al. 2016. "An Efficient Virus-Induced Gene Silencing Vector for Maize Functional Genomics Research." *Plant Journal* 86: 102–115.

Wu, C., L. Jia, and F. Goggin. 2011. "The Reliability of Virus-Induced Gene Silencing Experiments Using Tobacco Rattle Virus in Tomato Is Influenced by the Size of the Vector Control." *Molecular Plant Pathology* 12: 299–305.

Yamamoto, K., D. Grzech, K. Koudounas, et al. 2021. "Improved Virus-Induced Gene Silencing Allows Discovery of a Serpentine Synthase Gene in *Catharanthus roseus*." *Plant Physiology* 187: 846–857.

Yan, H., Z. Zhang, J.-L. Magnard, B. Boachon, S. Baudino, and K. Tang. 2020. "Virus-Induced Gene Silencing in Rose Flowers." *Methods in Molecular Biology* 2172: 223–232. Springer US.

Yang, W., L. Niu, Z. Xin, and Y. Zhang. 2025. "The Trihelix Transcription Factor PrASR3 Regulates α-Linolenic Acid Accumulation in Tree Peony Seeds." *Plant Journal* 124: e70546.

Zhan, J., and B. C. Meyers. 2023. "Plant Small RNAs: Their Biogenesis, Regulatory Roles, and Functions." *Annual Review of Plant Biology* 74: 21–51.

Zhang, Z., D.-W. Li, J.-H. Jin, et al. 2015. "VIGS Approach Reveals the Modulation of Anthocyanin Biosynthetic Genes by CaMYB in Chili Pepper Leaves." *Frontiers in Plant Science* 6: 500.

Zulfiqar, S., M. A. Farooq, T. Zhao, et al. 2023. "Virus-Induced Gene Silencing (VIGS): A Powerful Tool for Crop Improvement and Its Advancement Towards Epigenetics." *International Journal of Molecular Sciences* 24, no. 6: 5608.

Supporting Information

Additional supporting information can be found online in the Supporting Information section. **Table S1:** Table of plasmids. **Table S2:** Table of statistics for Figure 1. **Table S3:** Table of statistics for Supplementary Figure 1. **Table S4:** Table of statistics for Figure 4. **Table S5:** Table of statistics for Supplementary Figure 3. **Table S6:** Table of statistics for Supplementary Figure 4. **Table S7:** Table of Agrobacterium strains. **Table S8:** Table of primers. **Table S9:** Table of statistics for outliers. **Figure S1: Virus-induced gene silencing of phytoene desaturase and pTRV capsid in comparison to uninfiltrated plant in leaves.** Expression levels of CoPDS genes and the pTRV capsid in pot marigold leaves 38 days after infiltration with VIGS vectors as determined by qRTPCR; $n \geq 7$. Statistical significance was determined by a Kruskal–Wallis test with a post hoc Dunn test into groupings represented with α or β (Supplemental Table 3). **Figure S2: GC–MS of sterol standards and associated mass spectra.** (A) GCMS Total Ion chromatogram (TIC) of trimethylsilyl (TMS) derivatized sterols including (1) B-sitosterol, (2) stigmasterol, and (3) campesterol. Sterols were kindly provided by Anne Osbourn, John Innes Centre, Norwich, UK. (B) Mass spectra for TMS derivatized sterols. **Figure S3: Sterol accumulation did not change after virus-induced gene silencing**

of phytoene desaturase in comparison to uninfiltrated plant in leaves. Quantification of campesterol, isofucosterol, β-sitosterol, and stigmasterol in plants with reduced CoPDS expression compared to uninfiltrated plants as determined by GCMS compared to an internal standard; $n \geq 7$. Statistical significance was calculated using a Student's *t*-test for campesterol, isofucosterol and stigmasterol. A Mann–Whitney *U* test was used to test for significance in β-sitosterol as it was not of equal variance (Supplemental Table 5). EV = empty vector (pTRV2-PDS:GFP).
Figure S4: Virus-induced gene silencing of phytoene desaturase in comparison to uninfiltrated plant in flowers. Expression levels of CoPDS genes in pot marigold flowers 66 days after infiltration with VIGS vectors as determined by qRT-PCR; $n \geq 7$. Statistical significance was determined by a Kruskal–Wallis test for CoPDS1 as the data was not normally distributed and ANOVA with post hoc Tukey test for CoPDS2 into groupings represented with α or β (Supplemental Table 6). EV = empty vector (pTRV2-PDS:GFP), EV:FT = empty vector flowering locus T fusion (pTRV2-PDS:GFP:FT). **Data S1:** Video showing injection of *Agrobacterium tumefaciens* culture into midrib veins of *C. officinalis*.